Chapter 2

A Cell-Based Model for Ionic Electrodiffusion in Excitable Tissue

Ada J. Ellingsrud[1], Cécile Daversin-Catty[1] and Marie E. Rognes[1]

Abstract This chapter presents the KNP-EMI model describing ion concentrations and electrodiffusion in excitable tissue. The KNP-EMI model extends on the EMI model by removing the assumption that ion concentrations are constant in time and space, and may as such be more appropriate in connection with modelling e.g. spreading depression, stroke and epilepsy. The KNP-EMI model defines a system of time-dependent, nonlinear, mixed dimensional partial differential equations. We here detail the derivation of the system and present a numerical example illustrating how ion concentrations evolve during neuronal activity.

2.1 Introduction and Motivation

In this chapter, we present an extension of the EMI model, presented in (11, Chapter 1), describing ion concentrations and electrodiffusion in excitable tissue. The EMI model is based on the assumption that intra- and extracellular ion concentrations are constant in time and space. This is often a good approximation, as ion concentrations in healthy tissue typically quickly return to base levels after neuronal activity due to cellular mechanisms such as e.g. membrane pumps and glial cell buffering. However, there are scenarios where this assumption is inadequate.

Several cerebral pathologies are associated with increased neuronal activity (3), such as e.g. seizures and epilepsy (10; 6; 1), stroke (17), and spreading depression (22). In particular, periods of neuronal hyperactivity can lead to substantial variations in extracellular ion concentrations. These variations will in turn (i) influence membrane reversal potentials and (ii) generate diffusive currents. Changes in the reversal potentials, caused by local ionic shifts, may affect the dynamical properties of the

[1]Simula Research Laboratory, Norway

A. Tveito et al. (eds.), *Modeling Excitable Tissue*, Simula SpringerBriefs on Computing 7, https://doi.org/10.1007/978-3-030-61157-6_2

neurons (12; 16; 24). On the other hand, diffusive currents, driven by ion concentration gradients, can shift the extracellular potential (8; 3). Mathematical models addressing the aforementioned phenomena and pathologies should therefore also account for ion concentrations, their spatial and temporal gradients and associated dynamics.

In this chapter, we derive a system of time-dependent, nonlinear partial differential equations describing the distribution and evolution of ion concentrations in a geometrically-explicit representation of the intra- and extracellular domains using the electroneutral Kirchhoff-Nernst-Planck (KNP) model (21). We will refer to this model as the KNP-EMI model, see also e.g. (5).

2.2 Derivation of the Equations

Let the computational domain Ω and subdomains Ω_i, Ω_e, and Γ be defined as in the previous chapter 1.1. For simplicity and clarity, we present the mathematical model for one intracellular region $\Omega_{i^1} = \Omega_i$ with membrane Γ below. We model a set K of intracellular and extracellular ion concentrations, and note that key ions in excitable tissue are potassium (K^+), sodium (Na^+), and chloride (Cl^-). For each ion species $k \in K$ and each region $r \in \{i, e\}$, we model the *ion concentrations* $c_r^k : \Omega_r \times (0,T] \to \mathbb{R}$ (mol/m^3), and *electrical potentials* $u_r : \Omega_r \times (0,T] \to \mathbb{R}$ (V), and additionally the *total transmembrane current density* $I_m : \Gamma \times (0,T] \to \mathbb{R}$ (A/m^2).

2.2.1 Equations in the Intracellular and Extracellular Volumes

In the EMI model, the free current densities $\mathbf{J}_i, \mathbf{J}_e$ (μA/cm^2), c.f. (1.4), are assumed to satisfy Ohm's law. To include diffusive ion effects, we instead assume that the free current density is composed of flux density contributions $\mathbf{J}_r^k$ (mol/(m^{2}s)) from different ions k as:

$$\mathbf{J}_r = \sum_{k \in K} F z^k \mathbf{J}_r^k \quad \text{in } \Omega_r, \tag{2.1}$$

where z^k is the valence of ion species k and F (C/mol) is Faraday's constant. Furthermore, we assume that ions can move by diffusion and/or in response to the electrical field as charged particles. Hence, the ion flux densities are modelled as the sum of two terms: (i) the ion concentrations that are transported via electrical potential gradients $\sigma_r^k \nabla u_r$ and (ii) the diffusive movement of ions due to ionic gradients $D_r^k \nabla c_r^k$:

$$\mathbf{J}_r^k = -\sigma_r^k \nabla u_r - D_r^k \nabla c_r^k \quad \text{in } \Omega_r, \tag{2.2}$$

where D_r^k (m^2/s) and σ_r^k denote the effective diffusion coefficient and the conductivity for ion species k in region r, respectively. The conductivity σ_r^k depends on the concentration of ion species k and the diffusion coefficient D_r^k in the following manner:

$$\sigma_r^k = \sigma_r^k(c_r^k) = \frac{D_r^k z^k}{\psi} c_r^k \quad \text{in } \Omega_r. \tag{2.3}$$

Here, the constant $\psi = RTF^{-1}$ combines Faraday's constant F, the absolute temperature T (K), and the gas constant R (J/(K mol)). Moreover, the bulk conductivity σ_r can be expressed as:

$$\sigma_r = \sigma_r(c_r^k) = \frac{F}{\psi} \sum_{k \in K} D_r^k c_r^k (z^k)^2 \quad \text{in } \Omega_r. \tag{2.4}$$

See e.g. (21) for a derivation of the conductivity (2.3) and the bulk conductivity (2.4). Comparing with (1.4) and (1.5), we note the dependency on the ion concentrations in the conductivity σ_r in (2.3), and the second term accounting for ion diffusion in (2.2).

As in Chapter 1, we stipulate that:

$$\nabla \cdot \mathbf{J}_i = 0 \quad \text{in } \Omega_i, \tag{2.5}$$

$$\nabla \cdot \mathbf{J}_e = 0 \quad \text{in } \Omega_e. \tag{2.6}$$

Finally, conservation of ions for the bulk of each region Ω_r gives that:

$$\frac{\partial [k]_i}{\partial t} + \nabla \cdot \mathbf{J}_i^k = 0 \qquad \text{in } \Omega_i, \tag{2.7}$$

$$\frac{\partial [k]_e}{\partial t} + \nabla \cdot \mathbf{J}_e^k = 0 \qquad \text{in } \Omega_e, \tag{2.8}$$

for $t \in (0, T]$.

2.2.2 Membrane Currents

We next turn to modelling the cell membrane currents and membrane potential across the interface Γ. As in Chapter 1, we introduce the membrane potential v as the jump in the electrical potential over the membrane:

$$v = u_i - u_e \qquad \text{on } \Gamma. \tag{2.9}$$

We also introduce the total membrane current as the combination of a capacitive current and ion specific currents:

$$I_m = I_{\text{cap}} + I_{\text{ion}} = C_m \frac{\partial v}{\partial t} + I_{\text{ion}}, \tag{2.10}$$

where the total channel current I_{ion} is the sum of the ion specific channel currents I^k_{ion}:

$$I_{\text{ion}} = \sum_{k \in K} I^k_{\text{ion}}, \quad I^k_{\text{ion}} = I^k_{\text{ion}}(v, c^k_\cdot, \ldots). \tag{2.11}$$

The channel currents I^k_{ion} are subject to modelling, and will be discussed briefly in Section 2.2.2.1.

Using our concepts, we have that the *total ionic current density* $I_m : \Gamma \times (0,T) \to \mathbb{R}$ (A/m^2) across the interface Γ (from the intracellular to the extracellular domain) is given by:

$$-F \sum_{k \in K} z^k \mathbf{J}^k_e \cdot \mathbf{n}_e = F \sum_{k \in K} z^k \mathbf{J}^k_i \cdot \mathbf{n}_i \equiv I_m. \tag{2.12}$$

It now remains to specify a set of interface conditions for the specific ion fluxes $\mathbf{J}^k_r \cdot \mathbf{n}_r$ for $r \in \{i, e\}$.

Here, we propose a heuristic approach via ion specific capacitive current modelling, and note that an alternative approach is presented in (15). As for the total current, we assume that the capacitive current can be represented as a sum of ion specific contributions:

$$I_{\text{cap}} = \sum_{k \in K} I^k_{\text{cap}}. \tag{2.13}$$

Without loss of generality, we let the ion specific capacitive current $I^k_{\text{cap},r}$ in region Ω_r at the interface Γ be some fraction α^k_r of the total capacitive current I_{cap}:

$$I^k_{\text{cap},r} = \alpha^k_r I_{\text{cap}}. \tag{2.14}$$

Specifically, we assume that:

$$\alpha^k_r = \frac{D^k_r (z^k)^2 [k]_r}{\sum_{l \in K} D^l_r (z^l)^2 [l]_r}, \tag{2.15}$$

and note that $\sum_{k \in K} \alpha^k_r = 1$ for $r \in \{i, e\}$. By the above definitions, (2.10) and (2.12), we let the intracellular and extracellular ion fluxes across the membrane be given by:

$$\mathbf{J}^k_i \cdot \mathbf{n}_i = \frac{I^k_{\text{ion}} + \alpha^k_i (I_m - I_{\text{ion}})}{F z^k}, \qquad -\mathbf{J}^k_e \cdot \mathbf{n}_e = \frac{I^k_{\text{ion}} + \alpha^k_e (I_m - I_{\text{ion}})}{F z^k}, \tag{2.16}$$

for $k \in K$.

2.2.2.1 Modelling Specific Ion Channels

The membrane channel currents $I^k_{\text{ion}}(v)$ for each ion species k are subject to modelling. These currents are typically expressed on the form:

$$I^k_{\text{ion}}(v) = g^k_L(v - E^k), \tag{2.17}$$

where g^k_L is the conductivity, and E^k is the ion specific reversal potential (or Nernst potential), given by:

$$E^k = \frac{RT}{z^k F} \ln \frac{c^k_e}{c^k_i}. \tag{2.18}$$

This Nernst potential depends on the concentration ratio, whereas the Nernst potential in models without explicit modelling of ion concentrations is constant. Typical models include synaptic input currents, passive neuronal leak channels, or e.g. the Hodgkin-Huxley model (9). For more details on membrane current models and modelling, see e.g. (18).

2.2.3 Summary of KNP-EMI Equations

The KNP-EMI model equations follow from inserting (2.1) into (2.5)–(2.6), combined with (2.7), (2.8), (2.9), (2.10), and (2.16), and read as follows.

For each ion species $k \in K$ and each region $r \in \{i, e\}$, find the *ion concentrations* $c^k_r : \Omega_r \times (0,T] \to \mathbb{R}$ (mol/m^3), the *electrical potentials* $u_r : \Omega_r \times (0,T] \to \mathbb{R}$ (V), and the *total transmembrane current density* $I_m : \Gamma \times (0,T] \to \mathbb{R}$ (A/m^2) such that[1]:

$$\nabla\cdot(F \sum_k z^k \mathbf{J}^k_r) = 0 \qquad \text{in } \Omega_r, \tag{2.19}$$

$$\frac{\partial c^k_r}{\partial t} + \nabla\cdot \mathbf{J}^k_r = 0 \qquad \text{in } \Omega_r, \tag{2.20}$$

$$-F \sum_k z^k \mathbf{J}^k_e \cdot \mathbf{n}_e = F \sum_k z^k \mathbf{J}^k_i \cdot \mathbf{n}_i \equiv I_m \qquad \text{at } \Gamma, \tag{2.21}$$

$$v = u_i - u_e \qquad \text{at } \Gamma, \tag{2.22}$$

$$\frac{\partial v}{\partial t} = \frac{1}{C_m}(I_m - I_{\text{ion}}) \qquad \text{at } \Gamma, \tag{2.23}$$

where the ion flux density $\mathbf{J}^k_r$ is given by (2.2), and I_{ion} is subject to modelling. A set of initial and boundary or compatibility conditions will close the system.

[1] Note that the additional negative signs in (2.19) and (2.21), compared with the corresponding equations in Chapter 1, result from our physically consistent definition of the ion flux density $\mathbf{J}^k_r$ as the negative gradient, cf. (2.2).

2.3 Numerical Solution of the KNP-EMI Equations

The KNP-EMI model defines a complicated system of time-dependent, nonlinear, mixed dimensional partial differential equations. The number of unknowns depends on the number of ion species modelled. Some of the variables exist in the intracellular and extracellular domains, while others live on the lower-dimensional membrane. This setting is numerically challenging and calls for advanced techniques.

To solve the KNP-EMI model numerically, one may consider a finite difference scheme to approximate the time derivatives, a linearization of ion flux densities $\mathbf{J}_r^k$ and fractions α_r^k, a splitting scheme to handle active ion channel current models, and a finite element discretization in space. Such a solution algorithm is detailed in (5), and we refer the reader to this description for further details.

2.4 Comparing KNP-EMI and EMI during Neuronal Hyperactivity

Neurons are negatively charged relative to their environment, with a resting membrane potential of about −70 mV. This resting potential is maintained by low concentrations of sodium ions (Na^+) and high levels of potassium ions (K^+) inside the cell (23). Action potentials (neuronal activity) are generated by the opening of sodium and potassium channels in the cell membranes. The ionic gradient will drive sodium into the cell and depolarize the cell membrane. Next, the potassium channels open causing an outflux of potassium which in turn repolarizes the cell.

As a result, there is a continuous need to pump potassium into the intracellular space and sodium out to the extracellular space to restore the electrochemical gradient across the cell membrane. One of the key mechanisms for this process is the Na/K/ATPase pump. The Na/K/ATPase pump actively transports 3 Na^+ ions out of the cell and 2 K^+ ions into the cell (7; 14; 20). Several pathologies are associated with increased neuronal activity, e.g. seizures and epilepsy (10; 6; 1), and spreading depression (22). In periods of neuronal hyperactivity, the Na/K/ATPase pumps may not be able to restore the concentrations to baseline levels. Consequently, the electrochemical gradients may be reduced, and silenced neuronal activity and cellular swelling may occur (13).

The ion concentration gradients observed during neuronal hyperactivity thus yields a suitable setting for illustrating differences between the KNP-EMI and the EMI frameworks. In particular, we compare the two frameworks both during normal neuronal activity (firing rate of 1 Hz) and during hyperactivity (firing rate of 50 Hz).

2.4.1 Model Parameters and Membrane Mechanisms

We consider two idealized axons, represented by two parallel, rectangular domains, surrounded by extracellular space in three dimensions. The diameter of each axon is $2.0 \cdot 10^{-7}$ m, and they are separated by $1.0 \cdot 10^{-7}$ m of extracellular space. Parameter values are as listed in Table 2.1. We refer to the supplementary code for a complete description of the model set-up (4).

KNP-EMI membrane mechanisms The membrane mechanisms in the KNP-EMI model, cf. (2.11), are modelled using the standard Hodgkin-Huxley model (9) combined with a model for the Na/K/ATPase pump (12), the KCC2 cotransporter (24) and the NKCC1 cotransporter (24). The Na/K/ATPase pump current I_{ATP} (A/m^2) is modelled as:

$$I_{\text{ATP}} = I_{\text{ATP}}(c_i^{\text{Na}}, c_e^{\text{K}}) = \frac{\hat{I}}{(1 + \frac{m_{\text{K}}}{c_e^{\text{K}}})^2 (1 + \frac{m_{\text{Na}}}{c_i^{\text{Na}}})^3}, \tag{2.24}$$

where $\hat{I}$ is the maximum pump strength and m_{K} and m_{Na} denote the pump threshold for extracellular potassium and intracellular sodium, respectively. Further, the transmembrane currents generated by the KCC2 cotransporter I_{KCC2} (A/m^2) and the NKCC1 cotransporter I_{NKCC1} (A/m^2) are modelled as:

$$I_{\text{KCC2}} = S_{\text{KCC2}} \ln(\frac{c_i^{\text{K}} c_i^{\text{Cl}}}{c_e^{\text{K}} c_e^{\text{Cl}}}), \tag{2.25}$$

$$I_{\text{NKCC1}} = S_{\text{NKCC1}} \frac{1}{1 + e^{16 - c_e^{\text{K}}}} (\ln(\frac{c_i^{\text{K}} c_i^{\text{Cl}}}{c_e^{\text{K}} c_e^{\text{Cl}}}) + \ln(\frac{c_i^{\text{Na}} c_i^{\text{Cl}}}{c_e^{\text{Na}} c_e^{\text{Cl}}})), \tag{2.26}$$

where S_{KCC2} and S_{NKCC1} are the maximal cotransporter strengths. Moreover, the cell is stimulated by prescribing a synaptic input I_{syn} of the form:

$$I_{\text{syn}}^k = g_{\text{syn}} H e^{\frac{t - t_0}{\alpha}} (v - E^k), \tag{2.27}$$

where α (s) is the synaptic time constant, H is the Heaviside function for a small region on the left side of the axons, and $g_{\text{syn}} = 1.25 \cdot 10^{-3}$ S/m^2. In summary, the membrane channel currents for sodium, potassium and chloride are modelled as:

$$\begin{aligned}
I_{\text{ion}}^{\text{Na}}(v, c_r^{\text{k}}) &= g_{\text{leak}}^{\text{Na}}(v - E^{\text{Na}}) + \bar{g}^{\text{Na}} m^3 h (v - E^{\text{Na}}) + 3 I_{\text{ATP}} + I_{\text{NKCC1}} + I_{\text{syn}}^{\text{Na}} \\
I_{\text{ion}}^{\text{K}}(v, c_r^{\text{k}}) &= g_{\text{leak}}^{\text{K}}(v - E^{\text{K}}) + \bar{g}^{\text{K}} n^4 (v - E^{\text{K}}) - 2 I_{\text{ATP}} + I_{\text{NKCC1}} + I_{\text{KCC2}} \\
I_{\text{ion}}^{\text{Cl}}(v, c_r^{\text{k}}) &= g_{\text{leak}}^{\text{Cl}}(v - E^{\text{Cl}}) - 2 I_{\text{NKCC1}} - I_{\text{KCC2}},
\end{aligned}$$

where, g_{leak}^k and $\bar{g}^k$ is the leak conductivity and the maximal conductivity for ion species k, respectively, the Nernst potential E^k for ion species k is as described in Section 2.2.2.1, and the gating variables m, h and n are described by the standard Hodgkin-Huxley ODEs, see e.g. (23) for details.

EMI membrane mechanisms For the EMI model, we apply the standard Hodgkin-Huxley model and stimulate the cell by prescribing an input current of the form (2.27); thus, the membrane channels currents are modelled as:

$$I_{\text{ion}}(v) = g_{\text{leak}}^{\text{Na}}(v - E^{\text{Na}}) + g_{\text{leak}}^{\text{K}}(v - E^{\text{K}}) + g_{\text{leak}}^{\text{Cl}}(v - E^{\text{Cl}}) + \bar{g}^{\text{Na}} m^3 h(v - E^{\text{Na}}) + \bar{g}^{\text{K}} n^4 (v - E^{\text{K}}) + I_{\text{ATP}} + I_{\text{syn}},$$

where E^{K}, E^{Na} and E^{Cl} are calculated by (2.18) with the initial values from the KNP-EMI model for the sodium and potassium concentrations. Similarly, the bulk conductivities σ_i and σ_e are calculated by (2.4), and the net current from the Na/K/ATPase pump I_{ATP} is given by (2.24). Finally, there is no contribution from KCC2 and NKCC1, as both cotransporters mediate ion transport without any net charge movement across the membrane.

Parameter	Symbol	Value	Unit	Reference
gas constant	R	8.314	J/(K mol)	(23)
temperature	T	300	K	(23)
Faraday's constant	F	$9.648 \cdot 10^4$	C/mol	(23)
membrane capacitance	C_m	0.02	F/m	(24)
Na^+ diffusion coefficient	D_r^{Na}	$1.33 \cdot 10^{-9}$	m^2/s	(23)
K^+ diffusion coefficient	D_r^{K}	$1.96 \cdot 10^{-9}$	m^2/s	(23)
Cl^- diffusion coefficient	D_r^{Cl}	$2.03 \cdot 10^{-9}$	m^2/s	(23)
intracellular immobile anions	c_i^{A}	110	mM	
extracellular immobile anions	c_e^{A}	10	mM	
valence of immobile anions	z_A	-1		
Na^+ leak conductivity	g_L^{Na}	0.281	S/m^2	*
K^+ leak conductivity	g_L^{K}	0.43	S/m^2	*
Cl^- leak conductivity	g_L^{Cl}	0.2	S/m^2	*
K^+ HH max conductivity	$\bar{g}^{\text{K}}$	360	S/m^2	(9)
Na^+ HH max conductivity	$\bar{g}^{\text{Na}}$	1200	S/m^2	(9)
maximum pump strength	$\hat{I}$	0.18	A/m^2	(24)
maximum KCC2 strength	S_{KCC2}	0.0034	A/m^2	*
maximum NKCC1 strength	S_{NKCC1}	0.023	A/m^2	*
ECS K^+ pump threshold	m_{K^+}	3	mM	*
ICS Na^+ pump threshold	m_{Na^+}	12	mM	*
synaptic time constant	α	$1.0 \cdot 10^{-3}$	s	
global time step	Δt	$1.0 \cdot 10^{-5}$	s	
local time step	Δt^*	$\Delta t/25$	s	
spatial resolution	$\Delta x = \Delta y$	$2.5 \cdot 10^{-7}$	m	

Table 2.1: The physical and model parameters used in the simulations. The values are collected from Sterratt et al. (23), Hodgkin et al. (9), Wei et al. (24), whereas the values marked with * are computed by a steady state estimation.

The initial conditions for the intra- and extracellular ion concentrations, the membrane potential and the gating variables are listed in Table 2.2. At the exterior boundary, we apply no flux boundary conditions for each ion species.

Parameter	Symbol	Value	Unit	Reference
initial intracellular Na^+ concentration	$c_i^{Na,0}$	18	mM	
initial extracellular Na^+ concentration	$c_e^{Na,0}$	120	mM	
initial intracellular K^+ concentration	$c_i^{K,0}$	80	mM	
initial extracellular K^+ concentration	$c_e^{K,0}$	4	mM	
initial intracellular Cl^+ concentration	$c_i^{Cl,0}$	7	mM	
initial extracellular Cl^+ concentration	$c_e^{Cl,0}$	112	mM	
initial membrane potential	v^0	$-67.74 \cdot 10^{-3}$	V	*
initial HH gating value (Na^+ activation)	m^0	$\frac{\alpha_m(v^0)}{\alpha_m(v^0)+\beta_m(v^0)}$	–	(9)
initial HH gating value (Na^+ inactivation	h^0	$\frac{\alpha_h(v^0)}{\alpha_h(v^0)+\beta_h(v^0)}$	–	(9)
initial HH gating value (K^+ activation)	n^0	$\frac{\alpha_n(v^0)}{\alpha_n(v^0)+\beta_n(v^0)}$	–	(9)

Table 2.2: Initial conditions. The initial ion concentrations are chosen such that the Nernst potentials are equal to those in the Hodgkin-Huxley model (9). The membrane potential is computed by a steady state estimation.

2.4.2 Results and Discussion

During normal activity, the KNP-EMI and the EMI models behave similarly, both for the membrane potential and the extracellular potential (Figure 2.1 A, B). The stimuli current depolarizes the membrane potential above the threshold for firing, and an action potential is initiated (Figure 2.1 A). Simultaneously, the extracellular potential decreases by ~ 0.13 mV, before quickly returning to baseline (Figure 2.1 B).

During hyperactivity, the KNP-EMI and EMI models differ (Figure 2.1 C, D, E, F). In both models, repeated action potentials are triggered. But, for the KNP-EMI model, we observe changes in the membrane potential between hyperpolarization phases. In particular, we conclude that the KNP-EMI membrane resting potential increases with repeated firing: after 5 action potentials (at $t = 90$ ms) the membrane potential has a minimum value of -75 mV, which is an 9% increase from the first action potential. Eventually, the membrane is depolarized to the point where action potentials can long longer be fired (Figure 2.1 E).

The observed changes are caused by alterations in the ion concentration gradients. For each action potential, the extracellular Na^+ concentration decreases by 0.15 mM

and the extracellular K^+ concentration increases by 0.16 mM (Figure 2.2 A, B). During normal activity (Figure 2.2 A, B), the ion concentrations will slowly be pumped back toward baseline levels, and the membrane potentials are not substantially affected by the small ion concentration changes. However, in the case of hyperactivity, the membrane mechanisms (i.e. pumps and cotransporters) are not able to keep up. Consequently, the extracellular Na^+ concentration will keep decreasing and the extracellular potassium will keep increasing, causing the cell to depolarize (Figure 2.2 C, D).

In the KNP-EMI model (Figure 2.2 A, B), we note that 7.92 % of the extracellular K^+ concentration is restored, and 7.3 % of the extracellular Na^+ concentration is restored after 100 ms. That is, the extracellular concentrations do not reach baseline levels within the simulation period. Other studies have reported that it takes on the order of minutes (0.5 minutes (19), 6 minutes (2)) before the concentrations return to baseline after neuronal activity.

2.5 Conclusions and Outlook

In this chapter, we have presented a mathematical model, the KNP-EMI model, for ionic electrodiffusion in excitable tissue with an explicit representation of the intracellular, extracellular and membrane domains. For further reading on methodological aspects, we refer to (5; 15) and references therein. This model extends on the EMI model presented in Chapter 1 and may be more accurate in situations with rapid and persistent changes in ion concentrations. Moreover, the KNP-EMI framework allows for modelling ligand-gated ion channels (e.g. NMDA receptors).

The complexity of the KNP-EMI system yields a number of numerical challenges. The mere number of unknowns result in large systems of equations calling for efficient solution techniques. The nonlinearities in the system can easily lead to non-convergence and thus call for robust algorithms. Moreover, the coupling of full and lower dimensional domains and fields calls for well-posed numerical methods together with suitable simulation software. Further, the system couples different time scales: from neuronal action potentials taking place at the microscale to the slower diffusion process. In short, modelling ionic electrodiffusion in the EMI setting is an area with vast opportunities for further research.

Acknowledgements The authors would like to thank Geir Halnes for useful discussions and Min Ragan-Kelley for technical assistance.

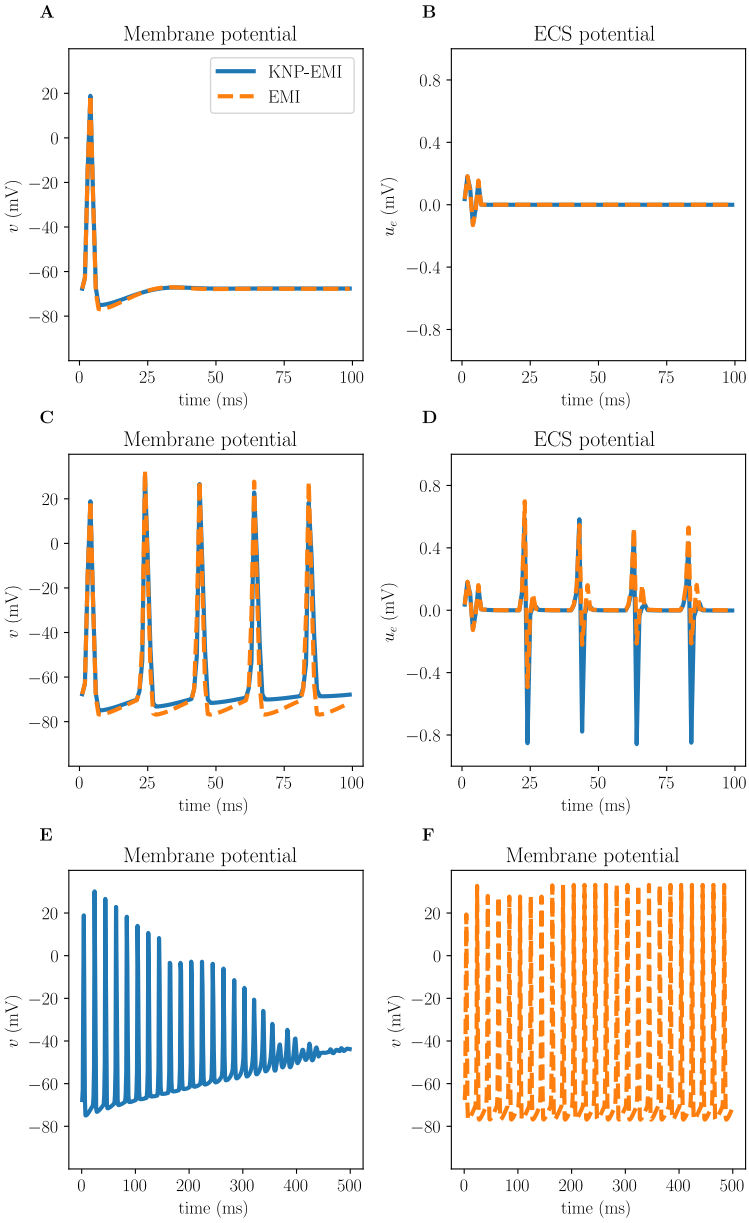

Fig. 2.1: Comparison of potentials over time at fixed points in space predicted by the KNP-EMI and the EMI frameworks during normal activity (upper panels) and during hyperactivity (mid and lower panels). The membrane potentials for KNP-EMI and EMI during normal activity (**A**) and hyperactivity (**C**, **E**, **F**), and the extracellular potentials for KNP-EMI and EMI during normal activity (**B**) and hyperactivity (**D**).

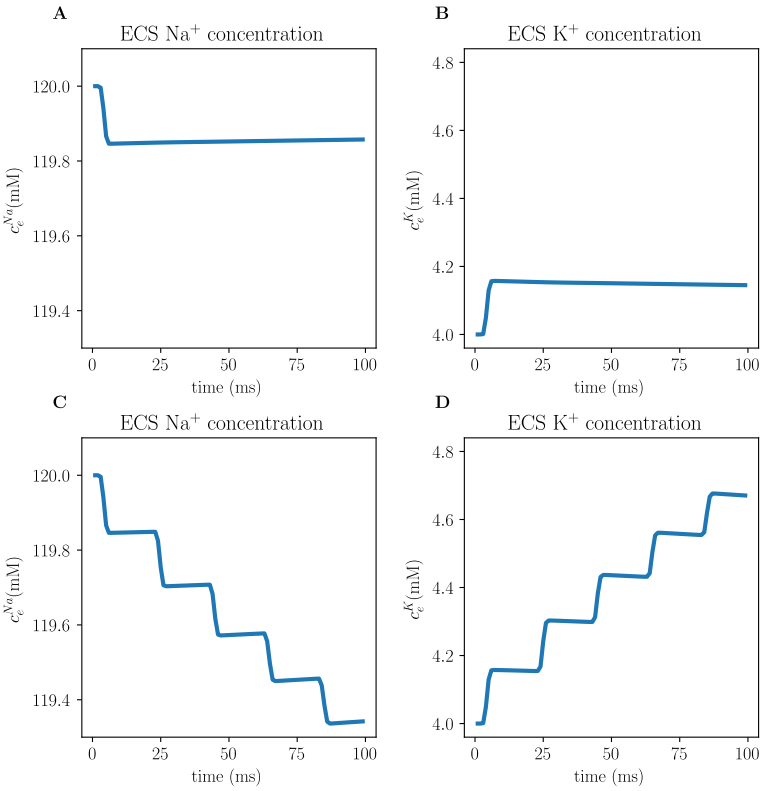

Fig. 2.2: Time development of extracellular ion concentrations at a fixed point in space for the KNP-EMI framework during normal activity (upper panels) and hyperactivity (lower panels). The extracellular sodium (**A**) and potassium (**B**) concentrations during normal activity, and the extracellular sodium (**C**) and potassium (**D**) concentrations during hyperactivity.

References

1. Bragin A, Engel Jr J, Wilson CL, Fried I, Mathern GW (1999) Hippocampal and entorhinal cortex high-frequency oscillations (100–500 Hz) in human epileptic brain and in kainic acid-treated rats with chronic seizures. Epilepsia 40(2):127–137
2. Chander BS, Chakravarthy VS (2012) A computational model of neuro-glio-vascular loop interactions. PloS one 7(11)
3. Dietzel I, Heinemann U, Lux H (1989) Relations between slow extracellular potential changes, glial potassium buffering, and electrolyte and cellular volume changes during neuronal hyperactivity in cat brain. Glia 2(1):25–44
4. Ellingsrud AJ (2020) Supplementary material (code) for Chapter 2 in 'EMI: Cell based mathematical model of excitable cells' (version 2.0). DOI 10.5281/zenodo.3767058, URL `http://doi.org/10.5281/zenodo.3767058`
5. Ellingsrud AJ, Solbrå A, Einevoll GT, Halnes G, Rognes ME (2020) Finite element simulation of ionic electrodiffusion in cellular geometries. Frontiers in Neuroinformatics 14:11
6. Fisher RS, Webber W, Lesser RP, Arroyo S, Uematsu S (1992) High-frequency EEG activity at the start of seizures. Journal of clinical neurophysiology: official publication of the American Electroencephalographic Society 9(3):441–448
7. Gadsby DC (2009) Ion channels versus ion pumps: the principal difference, in principle. Nature reviews Molecular cell biology 10(5):344–352
8. Halnes G, Mäki-Marttunen T, Keller D, Pettersen KH, Andreassen OA, Einevoll GT (2016) Effect of ionic diffusion on extracellular potentials in neural tissue. PLoS computational biology 12(11):e1005193
9. Hodgkin AL, Huxley AF (1952) A quantitative description of membrane current and its application to conduction and excitation in nerve. The Journal of physiology 117(4):500–544
10. Jacobs J, LeVan P, Chander R, Hall J, Dubeau F, Gotman J (2008) Interictal high-frequency oscillations (80–500 Hz) are an indicator of seizure onset areas independent of spikes in the human epileptic brain. Epilepsia 49(11):1893–1907
11. Jæger KH, Tveito A (2020) Derivation of a cell-based mathematical model of excitable cells. In: Tveito A, Mardal KA, Rognes ME (eds) Modeling excitable tissue - The EMI framework, Simula Springer Notes in Computing, SpringerNature
12. Kager H, Wadman WJ, Somjen GG (2000) Simulated seizures and spreading depression in a neuron model incorporating interstitial space and ion concentrations. Journal of neurophysiology 84(1):495–512
13. Kempski O (2001) Cerebral edema. In: Seminars in nephrology, Elsevier, vol 21, pp 303–307
14. de Lores Arnaiz GR, Ordieres MGL (2014) Brain Na+, K+-ATPase activity in aging and disease. International journal of biomedical science: IJBS 10(2):85

15. Mori Y, Peskin C (2009) A numerical method for cellular electrophysiology based on the electrodiffusion equations with internal boundary conditions at membranes. Communications in Applied Mathematics and Computational Science 4(1):85–134
16. Øyehaug L, Østby I, Lloyd CM, Omholt SW, Einevoll GT (2012) Dependence of spontaneous neuronal firing and depolarisation block on astroglial membrane transport mechanisms. Journal of computational neuroscience 32(1):147–165
17. Rabiller G, He JW, Nishijima Y, Wong A, Liu J (2015) Perturbation of brain oscillations after ischemic stroke: a potential biomarker for post-stroke function and therapy. International journal of molecular sciences 16(10):25605–25640
18. Rudy Y (2012) From genes and molecules to organs and organisms: heart. Comprehensive Biophysics pp 268–327
19. Sætra MJ, Einevoll GT, Halnes G (2020) An electrodiffusive, ion conserving Pinsky-Rinzel model with homeostatic mechanisms. bioRxiv
20. Scheiner-Bobis G (2002) The sodium pump. European Journal of Biochemistry 269(10):2424–2433
21. Solbrå A, Wigdahl BA, van den Brink Jonas, Anders MS, T EG, Geir H (2018) A Kirchhoff-Nernst-Planck framework for modeling large scale extracellular electrodiffusion surrounding morphologically detailed neurons. PLOS Computational Biology 14(10):1–26, DOI 10.1371/journal.pcbi.1006510, URL https://doi.org/10.1371/journal.pcbi.1006510
22. Somjen GG (2001) Mechanisms of spreading depression and hypoxic spreading depression-like depolarization. Physiological reviews 81(3):1065–1096
23. Sterratt D, Graham B, Gillies A, Willshaw D (2011) Principles of computational modelling in neuroscience. Cambridge University Press
24. Wei Y, Ullah G, Schiff SJ (2014) Unification of neuronal spikes, seizures, and spreading depression. Journal of Neuroscience 34(35):11733–11743